Title

A robust method for transfection in choanoflagellates illuminates their cell biology and the ancestry of animal septins

Short Title

Robust transfection in choanoflagellates

Authors

David S. Booth[1], Heather Szmidt-Middleton, and Nicole King[2]*

Howard Hughes Medical Institute and Department of Molecular and Cell Biology
University of California, Berkeley
Berkeley, CA 94720

[1] https://orcid.org/0000-0002-4724-4702

[2] https://orcid.org/0000-0002-6409-1111

*Corresponding author
Email: nking@berkeley.edu
Phone: (510) 643-9395

Keywords

choanoflagellates, transfection, animal origins, septin

Significance Statement

As the closest living relatives of animals, choanoflagellates provide unique insights into animal origins and core mechanisms underlying animal cell biology. However, unlike classic model organisms like yeast, flies, and worms, choanoflagellates have been refractory to DNA delivery methods for easily expressing foreign genes. Here we report a new approach to express proteins of interest in choanoflagellates. By engineering a panel of fluorescently-tagged proteins, we visualized choanoflagellate organelles in live cells and found that a class of cytoskeletal proteins called septins localizes to the basal poles of cells in choanoflagellates and animals. This approach opens the door to exploring gene function in choanoflagellates in greater detail and promises to illuminate the ancestry of animal cell biology.

Abstract

Choanoflagellates have the potential to be important experimental models due to their close relationship to animals, ability to develop into multicellular 'rosettes' that resemble animal embryos, ecological importance as bacterial predators, and responses to cues from environmental bacteria. Because choanoflagellates and animals share cellular features and gene families that are apparently absent from all other lineages, choanoflagellates provide unique insights into animal cell biology. However, choanoflagellates as experimental models have been limited by the absence of methods for transgene expression. Here we report a new and robust method for delivering and expressing transgenes in the choanoflagellate *Salpingoeca rosetta*, overcoming barriers that have previously hampered DNA delivery and expression. To demonstrate how this method offers new opportunities to investigate the cell biology of choanoflagellates, we engineered a panel of fluorescent protein markers that illuminates the subcellular architecture of live *S. rosetta* cells. These markers enabled the first *in vivo* characterization of choanoflagellate septins, cytoskeletal proteins that are hypothesized to regulate rosette development in *S. rosetta*. We show that septins localize to the basal pole of cells in *S. rosetta* rosettes in a pattern resembling septin localization in animal epithelia, revealing a likely cellular context of septin function in the first animals. This study advances the tractability of *S. rosetta* as an experimental model to investigate the molecular basis of choanoflagellate biology, core mechanisms underlying animal cell biology, and the origin of the first animals.

Introduction

First described in the mid-19th century, choanoflagellates inspired great debate regarding animal taxonomy (1). The most diagnostic morphological feature of choanoflagellates, a "collar complex" composed of a single apical flagellum surrounded by a collar of actin-filled microvilli (Fig. 1B), was interpreted as evidence of a special relationship between choanoflagellates and sponges, whose choanocytes (or "collar cells") each bear a collar complex (1). Subsequent phylogenetic analyses and the discovery of cells with a collar complex in nearly all animal phyla have revealed that sponges and all other animals are monophyletic, with choanoflagellates as their closest living relatives (Fig. 1)(2-6). Moreover, comparative genomic analyses have revealed that choanoflagellates, animals, and other holozoans express genes required for animal multicellularity and embryogenesis (7), including cadherins (8), tyrosine kinases (9, 10), and Myc (11); an additional ~896 gene families, including Notch, Delta, Flamingo, and protocadherins are exclusively shared by choanoflagellates and animals (12). Thus, comparisons among animals and choanoflagellates have the potential to provide unique insights into animal origins and core features of animal cell biology that are not conserved in other experimental models, such as yeast (13).

The choanoflagellate *Salpingoeca rosetta* (previously named *Proterospongia* sp. (14)) is emerging as an experimentally tractable model. *S. rosetta* develops from a single founding cell into a spherical, multicellular "rosette" (Fig. 1C) through serial rounds of cell division in a process that evokes the earliest stages of animal embryogenesis (15). Since the establishment of the first *S. rosetta* cultures in February 2000, *S. rosetta* has become increasingly amenable to cell and molecular biological approaches due to the sequencing of its genome (2), the establishment of forward genetic screens (16, 17), the ability to experimentally control key events in its life history (18), and the discovery that environmental bacteria induce rosette development and mating (18-21).

An important remaining barrier to the study of molecular and cellular mechanisms in *S. rosetta* has been the absence of techniques for transfection and transgene expression. Prior attempts at transgene delivery and expression have been unsuccessful, and the absence of the RNA interference pathway in *S. rosetta* prevents gene knockdowns (2, 12). Here we report the establishment of a robust nucleofection-based method to transfect *S. rosetta*. By engineering plasmids with *S. rosetta* regulatory sequences driving the expression of fluorescently-tagged *S. rosetta* proteins, we have developed a broad panel of markers for the study of choanoflagellate cell biology *in vivo*. As a proof of principle, we used transgene expression to characterize septins, genes with conserved roles in fungal (22, 23) and animal development (2, 24-27), that have been hypothesized to regulate rosette development (2). By imaging fluorescently-tagged septins in live cells, we show that their localization in *S. rosetta* resembles that in animal epithelia,

87 providing a potential evolutionary link between the mechanisms underlying animal and choanoflagellate
88 multicellularity.

Results

A robust method to transfect *S. rosetta*

To detect successful transfection, we started by engineering four different DNA plasmid constructs, each with different *S. rosetta* regulatory sequences fused to a gene, *nanoluc* (28), encoding a highly sensitive luciferase (Fig. S1B). Because no choanoflagellate promoters had previously been mapped, we fused *nanoluc* to non-coding sequences flanking *elongation factor L (efl)*, *α-tubulin (tub)*, *non-muscle actin (act)*, and *histone H3 (H3)*, each of which exhibit high expression, lack introns in their open reading frames and have well-annotated 5'- and 3'-untranslated regions (Fig. S1A) (2). Through this strategy, we aimed to increase the likelihood of cloning sequences that would drive robust *nanoluc* expression.

Next, we set out to deliver these DNA plasmid constructs into *S. rosetta* cells using nucleofection, an electroporation-based technique that has proven particularly effective for transfection of diverse eukaryotes (29-31), including mammalian primary cells that are resistant to transfection (32, 33). To quantify transfection efficiency, we performed luciferase assays on cell lysates. Although initial attempts at transfecting *S. rosetta* by nucleofection were not successful, we eventually achieved a low level of transfection with nucleofection by improving conditions for culturing *S. rosetta* cells (Fig. S2), modifying approaches for handling cells throughout the nucleofection procedure, and screening thirty unique combinations of electrical pulses and buffers (Fig. S3).

Optimization around these initial conditions culminated in a procedure that provided robust and reproducible transfection of *S. rosetta* (Fig. 2A; see Methods and http://www.protocols.io/groups/king-lab). When used in the optimized transfection procedure, all four transfection reporters drove strong expression of nanoluc protein, producing luminescence signals that were over three orders of magnitude above the detection limit (Fig. 2B).

Because this was the first example, to our knowledge, of successful transgene expression in any choanoflagellate, we sought to identify which steps in the optimized protocol were most essential. Using the p*H3-nanoluc* transfection reporter, we quantified how the omission of each step impacted transfection efficiency (Fig. 2C). In addition to the use of an optimal electrical pulse during nucleofection, the two most important steps were priming the cells through the enzymatic removal of the extracellular matrix prior to nucleofection (Fig. 2A, step 1; Fig. S4) and the inclusion of carrier DNA during nucleofection (Fig. 2A, step 2; Fig. S5); eliminating either of these steps resulted in a nearly complete loss of signal.

Priming the cells for nucleofection was a novel step motivated by our observation that *S. rosetta* cells are surrounded by a potentially protective extracellular coat (1, 17, 18), and the inclusion of carrier DNA (pUC19) in nucleofection reactions eliminated the need to include large quantities of reporter construct plasmid (Fig. S5). Another improvement was the development of a recovery buffer that

122 enhanced transfection ten-fold, presumably by promoting membrane resealing after nucleofection (34,
123 35).
124 Luciferase assays performed on cell lysates gave a sensitive read-out of population-wide nanoluc
125 expression but did not allow the examination of live, transfected cells nor reveal the proportion of cells
126 that were successfully transfected. Therefore, we next engineered eight reporters with different
127 fluorescent proteins placed under the control of regulatory sequences from the *S. rosetta actin* homolog.
128 Fluorescence was readily detected from cells transfected with reporters encoding mTFP1 (36), mWasabi
129 (37), sfGFP (38), mNeonGreen (39), mPapaya (40), TagRFP-T (41), mCherry (42), and tdTomato (42). In
130 contrast, an eGFP (43) reporter failed to yield fluorescent cells, likely due to protein misfolding, as cells
131 transfected with the 'super-folder' variant of GFP (sfGFP) did fluoresce properly. In transfected cells, the
132 fluorescent signal was distributed throughout the nucleus and cytosol yet excluded from membrane bound
133 compartments (Fig. 3A).
134 We observed that transfected cells resembled untransfected cells in their shape, motility, and ability
135 to propagate, indicating that transfection did not irreparably harm *S. rosetta*. Fluorescence persisted
136 through multiple cell divisions, yet the diminishing signal in daughter cells indicated that transfection was
137 transient (Fig. S6A) Importantly, using flow cytometry one to two days after transfection, we found that
138 ~1% of the population was reproducibly transfected, and fluorescence-activated cell sorting could isolate
139 this transfected cell population (Fig. S6B). This transfection frequency is comparable to high frequency
140 episomal transformation of the model yeast *Saccharomyces cerevisiae* that ranges from 1 – 10% (44, 45),
141 and similar transfection frequencies are achieved in model apicocomplexans (30, 46).
142
143 **Fluorescent markers illuminate the cell architecture of *S. rosetta***
144 The ability to express fluorescent proteins in *S. rosetta* provided a new opportunity to explore its
145 cell biology *in vivo*. Therefore, we designed a set of fluorescent reporters to mark key features of *S.*
146 *rosetta* cells: the nucleus, cytoplasm, collar, filopodia, flagellum, membrane, mitochondria and
147 endoplasmic reticulum (ER). For each fluorescent reporter, the *mCherry* gene was fused in-frame to *S.*
148 *rosetta* DNA sequences encoding conserved proteins or peptides that localize to specific organelles or
149 subcellular regions in yeast and mammalian cells. To benchmark each fluorescent marker, we compared
150 its localization in transfected cells to cellular landmarks known from electron and immunofluorescence
151 micrographs (Fig. S7) (1, 3, 8, 47, 48).
152 Electron micrographs have revealed two distinct regions in the nucleus: the darkly-stained
153 nucleolus positioned in the center and the surrounding, more lightly-stained nucleoplasm (1, 49). As
154 predicted, mCherry fused to either the carboxy terminus of H3 or the amino terminus of the simian virus
155 40 nuclear localization signal localized primarily to the *S. rosetta* nucleoplasm and was excluded from

156 both the nucleolus and the cytoplasm (Fig. 3B, C) (50, 51). In contrast, the cytoplasmic marker EFL-
157 mCherry (52) localized to the cytosol and was excluded from the nucleus (Fig. 3D).
158 Two of the most diagnostic features of the choanoflagellate cell are the actin-filled collar and the
159 flagellum, which is comprised of microtubules. A fusion of mCherry to the filamentous actin-binding
160 peptide Lifeact (53) highlighted the parallel arrangement of straight microvilli in the collar (Fig. 3G and
161 3J), as well as filopodia extending from the basal pole of the cell (Fig. 3G, lower arrow) (48). In live cells,
162 Lifeact-mCherry revealed the native structure of the collar, which can be distorted in cells fixed for
163 staining with fluorescent phalloidin or actin antibodies (48). Lifeact-mCherry also showed details of actin
164 filament organization that have not previously been evident, such as the existence of actin filaments that
165 originate in the cell body and coalesce at the base of the collar to form each microvillus (Fig. 3G', upper
166 arrow; improved immunofluorescence techniques also preserve these cortical actin filaments, Fig. 1B). A
167 fusion of α-tubulin to mCherry (54) illuminated individual cortical microtubules emanating from the base
168 of the flagellum to the basal pole of the cell (Fig. 3H', arrow) and allowed visualization of the rapidly
169 beating flagellum in live cells (Fig. 3H and 3K).
170 A cell membrane marker, with a geranyl-geranylation sequence fused to mCherry (55, 56), outlined
171 the entire cell, including the flagellum, collar, and cell body (Fig. 3I and 3L), and faintly marked the
172 Golgi apparatus (Fig. 3I', arrow). In live cells, the cell membrane marker captured the formation of a
173 phagocytic cup engulfing bacterial prey (Fig. S8)(57). The ER marker (58), which included the amino
174 terminal signal sequence from the secreted protein Rosetteless (17) and a carboxy terminal ER retention
175 sequence from the ER resident chaperone BiP (PTSG_07223), highlighted the continuity of the ER with
176 the nuclear envelope and the distribution of ER throughout the cell, including around vacuoles (Fig. 3F).
177 A mitochondrial marker (58) with an amino terminal targeting sequence from *S. cerevisiae* Cox IV
178 revealed a network of mitochondria (59) that is enriched around the nucleus and extends throughout the
179 cell (Fig. 3G). Taken together, these fluorescent markers provide the opportunity to investigate the
180 subcellular architecture of live *S. rosetta* cells in detail.
181
182 **Transgenesis reveals septin localization in live *S. rosetta* cells**
183 The establishment of transgenics in *S. rosetta* reported here will facilitate more rapid
184 characterization of candidate genes for multicellularity. As a demonstration of the utility of transgenic
185 approaches in *S. rosetta*, we investigated the localization of septins, a family of paralogous genes, each
186 encoding a protein with a diagnostic amino terminal guanosine triphosphate binding domain (G-domain)
187 and a carboxy terminal coiled-coil domain in most homologs (60, 61) (Fig. 4A). Septin paralogs interact
188 through their G-domains to form heteromeric filaments, and these heteromeric filaments interact with
189 each other through the septin coiled-coil domains to form higher order assemblies (62-64). The assembly

190 of septin filaments into higher order structures is important for proper septin localization (65), conserved
191 functions of septins in cytokinesis, and cell polarity in fungi and animals. Septins also serve more animal-
192 specific roles in phagocytosis (66), ciliogenesis (67), and planar cell polarity (27) . In the context of *S.*
193 *rosetta* biology, septins are particularly interesting because their mRNA abundance is elevated in
194 multicellular chain and rosette colonies relative to solitary swimming cells and they have been
195 hypothesized to contribute to rosette development (2).
196 We first examined the localization of the *S. rosetta* septin protein *Sr*Septin2 (PTSG_07215) with an
197 amino terminal mTFP1 tag in single cells and multicellular rosettes (Fig. 4B). Because septins visualized
198 by immunofluorescence microscopy in yeast (68-71), *Drosophila* (24, 25, 72), and mammalian cells (73)
199 display the same localization as septins tagged with fluorescent proteins, we reasoned that mTFP1-
200 *Sr*Septin2 should reveal the native localization of *Sr*Septin2 in *S. rosetta*. Strikingly, mTFP1-*Sr*Septin2
201 was enriched at the basal poles of single and rosettes cells (Fig. 4B and 4E) and at intercellular contacts
202 between adjacent cells in rosettes (Fig. 4E). Moreover, a separate *S. rosetta* septin, *Sr*Septin6
203 (PTSG_06009), displays the same basal localization as *Sr*Septin2 (Fig. 4C and Fig. S9), consistent with
204 the assembly of *Sr*Septin2 and *Sr*Septin6 into heteromeric filaments resembling those reported in yeast
205 and animals (64). We further found that the basal localization of *Sr*Septin2 requires the coiled-coil
206 domain, as a complete deletion of the coiled-coil domain (SrSeptin2ΔCC; Fig. 4A, D, F) eliminated
207 *Sr*Septin2 enrichment at the basal pole when expressed in wild-type cells. Unexpectedly, mTFP1-
208 *Sr*Septin2ΔCC formed ectopic rings around vesicles in the cytosol in wild-type cells (Fig. 4D and 4F).
209 The basal and lateral localization of *Sr*Septin2 and *Sr*Septin6 in rosettes is reminiscent of septin
210 localization in polarized epithelial cells (73, 74), in which septins interact with the positive ends of
211 microtubules that are growing toward the basal pole (75). In choanoflagellates, microtubules radiate down
212 from the apical microtubule organizing centers, with the plus ends meeting at the basal pole of each cell,
213 similar to the orientation of microtubule plus ends toward the basal pole in animal epithelia (76). To
214 examine if septins also interact with the plus ends of microtubules in *S. rosetta*, we co-transfected cells
215 with mTFP1-*Sr*Septin2 and the tubulin marker α-tubulin-mCherry (Fig. 4G). Fluorescence microscopy
216 showed that septin filaments intercalate between cortical microtubules at the basal pole of the cell (Fig.
217 4G). These data are consistent with conserved interactions between septins and microtubules from yeast
218 to animals (77), including at the plus-ends of microtubules in choanoflagellates and animal epithelia.
219

Discussion

By synthesizing our growing knowledge of *S. rosetta* biology with a rigorous characterization and optimization of each step in the transfection procedure, we have developed a robust method for transgenesis in *S. rosetta* that can be easily implemented by other laboratories. This method overcomes the barriers that prevented efficient DNA delivery in our prior attempts using diverse methods, including standard electroporation, lipofection, bombardment, and cell-penetrating peptides. A key breakthrough for this study was the realization that the extracellular coat surrounding *S. rosetta* might present a barrier for transfection, which motivated the development of a method to gently remove the extracellular material surrounding *S. rosetta,* thereby sensitizing cells for transfection. Additional improvements to the transfection procedure, such as a step for promoting the closure of the plasma membrane after electrical pulsation, were designed to address the unique challenges that arise from culturing *S. rosetta* in sea water. Just as our method was informed by approaches developed in model microeukaryotes (*Chlamydomonas* and yeast), the methods we have established in *S. rosetta* may extend to aid gene delivery in diverse non-model marine microeukaryotes. Overall, the gestalt of continually improving choanoflagellate husbandry (16), developing protocols for priming and recovering cells during nucleofection, and extensively optimizing transfection based on a quantitative assay produced a robust method for gene delivery in *S. rosetta*.

This work also provides a foundational set of vectors for expressing transgenes in *S. rosetta* (Dataset S1). In these vectors, the expression of luciferase or fluorescent proteins was placed under the control of native regulatory elements. From these vectors, we constructed a panel of fluorescently tagged subcellular markers that serve as fiducial markers for monitoring the localization of proteins in *S. rosetta*. For example, through our pilot study of *Sr*Septin2 and *Sr*Septin6, the use of these new transgenic tools revealed that septins localize to the basal pole of choanoflagellates, mirroring their localization in animal epithelial cells (73, 74). This observation provides a valuable intermediate for understanding how septin functions evolved prior to the evolution of an epithelium in stem animals. While septins have broadly conserved roles in cytokinesis and cell polarity, the specifics differ between fungi and animals, which diverged over a billion years ago and have important differences in their cell biology. In yeast, septins facilitate polarized cell growth toward the new daughter cell prior to mediating cytokinesis. In animals, septins not only facilitate cytokinesis (78) but also maintain apical-basal and planar cell polarity to properly coordinate multicellular development (25, 27, 74). The basal localization of septins in choanoflagellates and animal epithelia suggests that septins played a role in apical-basal polarity evolved before the divergence of choanoflagellates and animals. Further insights into the ancestral functions of septins are likely to emerge through continued study in *S. rosetta* and through the study of septin function

253 in other non-metazoan holozoans, including *Capsaspora owczarzaki* (79) and *Creolimax fragrantissima*
254 (80), in which transgenic methods have also been recently established.
255 Previous analyses of gene function in choanoflagellates relied on custom antibodies (8, 11, 17, 49),
256 laborious forward genetic screens (17), and *in vitro* biochemistry (49). The establishment of transgene
257 expression in *S. rosetta* described here will accelerate studies of the ancestral functions of animal genes
258 that are conserved in choanoflagellates. We anticipate that future work will build on this approach to
259 establish stable transgenesis and genome editing. Establishing reverse genetics tools will likely require an
260 increased understanding of choanoflagellate DNA recombination and repair as well as the development of
261 quantitative genotyping assays optimized for choanoflagellates. Combining an expanded repertoire of
262 approaches for investigating gene function in-depth in *S. rosetta* with comparisons to other
263 experimentally-tractable choanoflagellates (12, 81) and non-choanozoans (79, 80) promises to yield
264 increasingly mechanistic insights into the ancestry of animal cell biology.
265

266 ## Materials and Methods

267

268 ### Cell culture and media preparation

269 *S. rosetta* was cultured with a single bacterial species, *E. pacifica*, that serves as a food source (16).
270 Media recipes are provided in Table S1. Cultures were established from frozen aliquots by adding 1 ml of
271 thawed cells to 10 ml of 0.2x High Nutrient Media. After the cells reached a density of 10^4 cells/ml, the
272 culture was split 1:2 into 1x High Nutrient Media with a constant volume of 0.24 ml/cm^2. After this initial
273 split (denoted as day 0), cells were passaged in 1x High Nutrient Media according to the following
274 schedule: 1:4 dilution on day 1, 1:8 dilution on day 2, 1:16 on day 3. Subsequently cells were passaged
275 every day at a 1:24 dilution or every other day as a 1:48 dilution of cells.

276 Based on the recommendation from Lonza to use a medium with a low calcium concentration for
277 transfecting mammalian cells, we searched for a seawater recipe with a lower concentration of calcium
278 than the routinely-used artificial seawater made from Tropic of Marin Salts (16), which has a calcium
279 concentration of 9.1 mM at a salinity of 35 g/kg (82). The AK seawater formulation that has been used to
280 culture marine algae (83) and dinoflagellates (84) and has a calcium concentration of 2.7 mM. We found
281 that *S. rosetta* grows more rapidly in 1x High Nutrient Media prepared in AK seawater rather than
282 seawater prepared with Tropic of Marin Salts (Fig. S2A). Therefore, we switched to a growth medium
283 based on AK seawater for routine culturing. After optimizing the nucleofection protocol, we
284 demonstrated that growing *S. rosetta* in AK seawater also resulted in higher transfection efficiencies (Fig.
285 S2B) than growing *S. rosetta* in seawater prepared with Tropic of Marin Salts.

286

287 ### Reporter plasmid design and molecular cloning

288 Dataset S1 lists the complete inventory of engineered plasmids with a summary of primers, cloning
289 methods, and annotations for constructing each plasmid. Complete plasmid sequences and plasmids have
290 also been deposited at Addgene (http://www.addgene.org/Nicole_King). Below is a brief summary of
291 considerations for designing plasmids, and a more detailed description of standard molecular cloning
292 methods for engineering plasmids can be found in the Supplementary Information.

293 **Cloning regulatory regions from *S. rosetta* genes.** Because we had no previous knowledge about
294 the architecture of choanoflagellate regulatory regions, we aimed to clone as much as 1000 bp upstream
295 and downstream of targeted open reading frames as these fragments are slightly larger than the mean
296 intergenic distance of 885 bp (7). Of necessity, the cloned intergenic sequences reported here were shorter
297 to avoid repetitive CA and GT sequences that were present before the putative promoter and after the 3'-
298 UTR, respectively. To increase the specificity of primers, we designed the primers to anneal to regions
299 with a GC content ≤ 50%, as the *S. rosetta* genome is 56% GC. Ultimately, the cloned regions that

300 encompass the promoter and the 5'-UTR ranged in size from 550 bp to 1095 bp and those encompassing
301 the 3'UTR ranged from 200 bp to 807 bp.
302 **Synthetic gene design.** Synthetic reporter genes (*nanoluc* and the genes encoding diverse
303 fluorescent proteins) were codon optimized to match the codon usage of the set of highly expressed
304 intron-less genes listed in Fig. S1, as codon usage can be biased for highly expressed genes (85). A codon
305 usage table (Dataset S2) was generated from the coding sequences of highly expressed intronless genes
306 (Dataset S2A) and from all coding sequences (Dataset S2B) using the 'cusp' tool in Emboss (86). The
307 codon usage table was then used to generate a codon optimized DNA sequence for each target protein
308 sequence with the 'backtranseq' tool on Emboss. The DNA sequences were further edited by making
309 synonymous substitutions with less frequently used codons to change restriction enzyme sites and to
310 remove repetitive sequences. Finally, sequences were added to the ends of these designed genes for
311 cloning with restriction enzymes or Gibson assembly. The engineered reporter gene sequences are
312 available through Addgene (Dataset S1; http://www.addgene.org/Nicole_King).
313 **Subcellular marker design.** Dataset S3 provides the amino acid sequences for all of the
314 subcellular markers reported in Fig. 3. To ensure that the fluorescent protein tag for each marker would
315 not interfere with the functions of proteins or peptides that determine localization, some of the constructs
316 were engineered to have a flexible linker sequence (SGGSGGS) separating the fluorescent protein and the
317 localization signals.
318
319 **Optimized transfection protocol**
320 The protocol is summarized in Fig. 2 and detailed protocols for reagent preparation and transfection are
321 available at protocols.io at the following link: http://www.protocols.io/groups/king-lab
322 **Culture.** Two days prior to transfection, a culture flask (Corning, Cat. No. 353144) was seeded
323 with *S. rosetta* at a density of 5,000 cells/ml in 200 ml of 1x High Nutrient Media. The culture was
324 supplemented with 2 mg of frozen *E. pacifica* by resuspending a 10 mg pellet of flash-frozen *E. pacifica*
325 in 1 ml of media and then adding 200 μl of the resuspended pellet to the culture of *S. rosetta*.
326 **Wash.** After 36-48 hours of growth, bacteria were washed away from *S. rosetta* cells through three
327 consecutive rounds of centrifugation and resuspension in sterile AK seawater. The culture flask was
328 vigorously shaken for 30 sec to homogenize the 200 ml that was seeded two days prior (see above) and
329 then transferred to 50 ml conical tubes and spun for 5 min at 2000 x g and 22°C. The supernatant was
330 removed with a serological pipette, and residual media was removed with a fine tip transfer pipette. The
331 cell pellets were resuspended in a total volume of 100 ml of AK seawater, vigorously shaken in their
332 conical tubes for 30 sec, and then centrifuged for 5 min at 2200 x g and 22°C. The supernatant was
333 removed as before. Each cell pellet was resuspended in 50 ml of AK seawater, vigorously shaken for 30

334 sec, and centrifuged for 5 min at 2400 x g and 22°C. After the supernatant was removed, the cells were
335 resuspended in a total volume of 100 μl of AK seawater. A 100-fold dilution of cells was counted on a
336 Luna-FL automated cell counter (Logos Biosystems) and the remaining cells were diluted to a final
337 concentration of $5x10^7$ choanoflagellate cells/ml. The resuspended cells were divided into 100 μl aliquots
338 with $5x10^6$ cells per aliquot to immediately prime cells in the next step. A 200 ml culture typically yields
339 6-8 aliquots of cells.

340 **Prime.** After washing away bacteria, each aliquot of *S. rosetta* cells was incubated in priming
341 buffer to remove the extracellular material coating the cell. The 100 μl aliquots that contained $5x10^6$ cells
342 were centrifuged for 5 min at 2750 x g at room temperature. The supernatant was removed with a fine tip
343 micropipette. Cells were resuspended in 100 μl of priming buffer (40 mM HEPES-KOH, pH 7.5; 34 mM
344 Lithium Citrate; 50 mM L-Cysteine; 15% (w/v) PEG 8000; and 1 μM papain) and then incubated for 30
345 min. Priming was quenched by adding 2 μl of 50 mg/ml bovine serum albumin-fraction V (Sigma) and
346 then centrifuged for 5 min at 1250 x g and 22°C with the centrifuge brake set to a 'soft' setting. The
347 supernatant was removed with a fine-tip micropipette, and the cells were resuspended in 25 μl of SF
348 Buffer (Lonza).

349 **Nucleofect.** Each transfection reaction was prepared by adding 2 μl of 'primed' cells resuspended
350 in SF buffer to a mixture of 16 μl of SF Buffer; 2 μl of 20 μg/μl pUC19; 1 μl of 250 mM ATP, pH 7.5; 1
351 μl of 100 mg/ml Sodium Heparin; and ≤7 μl of reporter DNA. (Note that higher volumes of nucleofection
352 lead to lower transfection frequencies; thus, reporter DNA should be as concentrated as possible, not
353 exceeding 7 μl. Also, see below for "Note about titrating reporter plasmids.") The transfection reaction
354 was transferred to one well of a 96-well nucleofection plate (Lonza). The nucleofection plate was placed
355 in a Nucleofector 4d 96-well Nucleofection unit (Lonza), and the CM156 pulse was applied to each well.

356 **Rest and recover.** Immediately after pulsation, 100 μl of ice-cold recovery buffer (10 mM HEPES-
357 KOH, pH 7.5; 0.9 M Sorbitol; 8% (w/v) PEG 8000) was added to the cells, Recovery buffer was gently
358 mixed with the transfected cells by firmly tapping the side of the plate and then incubating the samples for
359 5 min. The whole volume of the transfection reaction plus the recovery buffer was transferred to 1 ml of
360 1x High Nutrient Media in a 12-well plate. After the cells recovered for 1 hour, 5 μl of a 10 mg frozen *E.*
361 *pacifica* pellet resuspended in media (see above), was added to each well. The cells were grown for 24 to
362 48 hours before assaying for luminescence or fluorescence.

363 **Note about establishing transfection in non-model microeukaryotes.** Establishing a transfection
364 protocol for *S. rosetta* required adapting several different transfection procedures for a variety of
365 eukaryotic cells to meet the unique requirements of *S. rosetta*. While the specific details for transfecting
366 *S. rosetta* may not be readily applicable to other organisms, the general considerations and the process for
367 optimization that led to the development of the transfection protocol described here could inform efforts

368 to transfect other microeukaryotes. Therefore, we have included a summary in the Supplementary Text
369 and Figs. S10 and S11 about the initial development and optimization of the aforementioned protocol.
370
371 **Nanoluc reporter assay**
372 To measure relative transfection efficiency resulting from different transfection protocols and
373 promoters, we performed luciferase assays on lysates of transfected cells. Cells transfected with 2.5 μg of
374 *nanoluc* reporter plasmids were pelleted by centrifuging for 10 min at 4200 x g and 4°C. The supernatant
375 was removed and the cells were resuspended in 50 μl of NanoGlo buffer (Promega) and then transferred
376 to a well of a white, opaque 96-well plate (Greiner Bio-one Cat No.655083). Luminescence was
377 immediately recorded on a Spectramax L Microplate Reader (Molecular Devices) with a 1 min dark
378 adaption and 10 sec dwell time with the photomultiplier gain set to photon counting mode.
379 Based on standard definitions from analytical chemistry (87) the detection limit was set to three
380 standard deviations above the background signal such that any signal above the detection limit has less
381 than a 1% chance of arising from random error. The limit of detection was calculated in two different
382 ways. First, the y-axis intercept and standard deviation were calculated from a standard curve (87) fit to a
383 serial dilution of nanoluc versus luciferase activity (Fig. S3A). To decrease the bias toward higher
384 luciferase values, the standard curve was fit with the objective *(O)*: $O \equiv \min \sum_i \frac{|m_i - c_i|}{m_i}$, where m is the
385 measured luciferase value for a given data point i and c is the calculated luciferase value. Second, the
386 detection limit was also determined as three standard deviations above the mean of eight replicate
387 luciferase measurements of cells transfected without any reporter plasmid, which resulted in the same
388 calculated detection limit.
389 Reproducibility in luciferase assays was assessed by performing at least two independent
390 experiments on separate days with different preparations of 'primed' cells; data presented in Fig. 2
391 represent one of the independent experiments. Within each experiment from the same preparation of
392 'primed' cells, replicate measurements were performed by setting up three to five independent
393 transfections for each condition (shown as black dots); bar graphs in Fig. 2 show the mean values of the
394 five independent transfections with error bars showing the standard deviation. Before performing
395 statistical tests that rely on a normal distribution, luciferase data were transformed to a log-normal
396 distribution by taking the base-10 logarithm of luciferase values as gene expression data from luciferase
397 assays display a log-normal distribution (88).
398
399 **Flow Cytometry**
400 To measure the percentage of cells expressing each of the different transgenes under different
401 transfection conditions, we used flow cytometry. Cells were transfected with 10 μg of mWasabi or 10 μg

402 of TagRFP-T reporter plasmids for flow cytometry because these fluorophores produced the highest
403 fluorescence signal upon illumination with the 488 or 561 nm lasers, respectively. To prepare cells for
404 flow cytometry, cultures from 10-12 transfections were pooled 24 hours after transfection and centrifuged
405 for 15 min at 3600 x g and 4°C. The supernatant was removed with a fine-tip transfer pipette to avoid
406 disturbing the pellet. The pelleted cells were resuspended in 500 μl of 0.22 μm filtered AK seawater and
407 then filtered through a 40 μm filter.

408 Because a large number of bacteria were present in the cultures, *S. rosetta* cells were gated based on
409 the area of forward scattering signal versus the area of the side scattering signal and the area of the
410 forward scattering signal versus the height of the forward scattering signals. To differentiate transfected
411 cells from untransfected cells, fluorescence signal was measured using lasers and filters for the
412 fluorophores FITC (Green Fluorescence) and PE (Red Fluorescence); untransfected cells form a
413 population along the y=x line of these plots, and the population of transfected cells are skewed along one
414 axis that corresponds to the fluorophore. The transfected cells were gated to exclude >99.99% of
415 untransfected cells as determined from a negative control reaction that was transfected without a
416 fluorescent reporter (Fig. 2E, left panel).
417
418 **Live cell imaging**

419 An important benefit of transgenics is the ability to visualize protein localization and cell
420 architecture in living cells. To this end, we have established improved protocols for live cell imaging in *S.*
421 *rosetta*. Glass-bottomed dishes were prepared for live cell microscopy by corona-treating the glass for 10
422 s. Afterwards, 300 μl of 0.1 mg/ml poly-D-lysine was applied to the glass cover (18 μl/cm^2), incubated
423 for 10 min at room temperature, and then removed. Excess poly-D-lysine was washed away from the
424 glass surface with three rinses of 500 μl artificial seawater.

425 Cells transfected with 5 μg of each fluorescent reporter were prepared for microscopy by
426 centrifuging 1-2 ml of transfected cells for 10 min at 3,600 x g and 4°C. After centrifugation, the
427 supernatant was removed and the cell pellet was resuspended in 200 μl of 4/5 Tropic of Marin artificial
428 seawater with 100 mM LiCl. Lithium chloride slows flagellar beating, as in spermatozoa (89, 90), to
429 decrease the movement of cells during imaging. The resuspended cells were pipetted on top of the poly-
430 D-lysine coated glass-bottom dish and adsorbed on the surface for 10 min. Lastly, 200 μl of 20% (w/v)
431 Ficoll 400 dissolved in 4/5 Tropic of Marin artificial seawater with 100 mM LiCl was pipetted drop-by-
432 drop on top of the cells. The addition of Ficoll decreases flagellar movement by increasing the viscosity
433 of the media (91, 92) without significantly changing the osmolarity or refractive index of the sample (GE
434 Lifesciences).

435 Confocal microscopy was performed on a Zeiss Axio Observer LSM 880 with an Airyscan detector
436 and a 63x/NA1.40 Plan-Apochromatic oil immersion objective. The mTFP1 and mCherry fluorophores
437 were selected for two-color imaging due to their high photostability and minimal spectral overlap.
438 Confocal stacks were acquired in superresolution mode using ILEX line scanning and two-fold averaging
439 and the following settings: 40 nm x 40 nm pixel size, 93 nm z-step, 0.9-1.0 μsec/pixel dwell time, 850
440 gain, 458 nm laser operating at 5% laser power, 561 nm laser operating at 3% laser power, 458/561 nm
441 multiple beam splitter, and 495-550 nm band-pass/570 nm long-pass filter. Images were initially
442 processed using the automated Airyscan algorithm (Zeiss) and then reprocessed by setting the Airyscan
443 threshold 0.5 units higher than the value reported from automated Airyscan processing. The stacks were
444 further processed by correcting for signal decay, background, and flickr in Zen Blue (Zeiss). Last, FIJI
445 (93) was used to apply a gamma factor to each channel and subtract the background using a 100 pixel
446 radius.
447 Epifluorescence and differential interference contrast images were recorded using a Zeiss Axio
448 Observer.Z1/7 Widefield microscope with a Hamamatsu Orca-Flash 4.0 LT CMOS Digital Camera and
449 40x/NA 1.1 LD C-Apochromatic water immersion, 63x/NA1.40 Plan-Apochromatic oil immersion, or
450 100x NA 1.40 Plan-Apochromatic oil immersion objectives. Green fluorescent proteins were imaged with
451 a 38 HE filter set and red fluorescent proteins with a 43 HE filter set. Images were processed by applying
452 a gamma factor and background subtracting fluorescence channels in FIJI.
453 **Note about titrating reporter plasmids.** A titration of fluorescent reporter plasmids showed that
454 10 μg of total reporter plasmid(s) best balanced transfection efficiency, brightness, and a faithful
455 indication of subcellular architecture. We caution that high plasmid concentrations can result in the
456 overexpression of fluorescent markers, leading to aberrant localization of the marker and gross changes in
457 cell morphology. Such artefacts can be avoided by performing a titration to determine the best
458 concentration of plasmid and recording images from cells with a range of fluorescence intensities that
459 result from any transfection. One of the best markers to assess optimal reporter plasmid concentrations is
460 the tubulin marker because of its distinct localization that can be benchmarked with immunofluorescence.
461
462 **Immunofluorescence staining and imaging**
463 Immunfluorescence was performed as previously described (20) with modifications to better
464 preserve features of the cytoskeleton. Two milliliters of cells were concentrated by centrifugation for 10
465 min at 2750 x g and 4°C. The cells were resuspended in 400 μl of artificial seawater and applied to poly-
466 L-lysine coated coverslips (BD Biosciences) placed in the bottom of each well of a 24-well cell culture
467 dish. After allowing the cells to settle on the coverslip for 30 min, 150 μl of the cell solution was gently
468 removed from the side of the dish. It is crucial to leave a small layer of buffer on top of cells to preserve

469 the cell morphology, hence the 250 μl of liquid left in the well. All of the subsequent washes and
470 incubations during the staining procedure were performed by adding and removing 200 μl of the indicated
471 buffer.
472 Cells were fixed in two stages. First, the coverslip was washed once with 6% acetone in
473 cytoskeleton buffer (10 mM MES, pH 6.1; 138 KCl, 3 mM $MgCl_2$; 2 mM EGTA; 675 mM Sucrose),
474 which better preserves the actin cytoskeleton (94, 95), and then incubated for 10 min at room temperature
475 after a second application of the acetone solution. Subsequently, the coverslip was washed once with 4%
476 formaldehyde diluted in cytoskeleton buffer and then incubated for 15 min at room temperature after a
477 second application of the formaldehyde solution. Last, the coverslip was gently washed three times with
478 cytoskeleton buffer.
479 Cells were permeabilized by washing the coverslip once with permeabilization buffer (100 mM
480 PIPES, pH 6.95; 2 mM EGTA; 1 mM $MgCl_2$; 1% (w/v) bovine serum albumin-fraction V; 0.3% (v/v
481 Triton X-100) and then incubated for 30 min upon a second addition of permeabilization buffer. After the
482 permeabilization buffer was removed, the coverslip was washed once with primary antibody, 50 ng/ml
483 mouse E7 anti-tubulin antibody (Developmental Studies Hybridoma Bank) diluted in permeabilization
484 buffer, and then incubated for 1 h in a second application of primary antibody. The coverslip was gently
485 washed twice in permeabilization buffer. Next, the coverslip was washed once with secondary antibody, 8
486 ng/ml Donkey anti-mouse IgG–AlexaFluor568 (ThermoFisher) diluted in permeabilization buffer, and
487 then incubated for 1 h after a second application of secondary antibody. Afterwards, the coverslip was
488 washed once in permeabilization buffer and then three times with PEM (100 mM PIPES-KOH, pH 6.95;
489 2 mM EGTA; 1 mM $MgCl_2$). The coverslip was washed once with 10 μg/ml Hoechst 33342 and 4 U/ml
490 Phalloidin-AlexaFluor488 in PEM and then incubated for 30 min with a second application of
491 Hoechst3334/Phalloidin. Finally, the coverslip was washed once in PEM.
492 To prepare a slide for mounting, 10 μl of Pro-Long Diamond (Invitrogen) was added to a slide. The
493 coverslip was gently removed from the well with forceps, excess buffer was blotted from the side with a
494 piece of filter paper, and the coverslip was gently placed on the drop of Pro-Long diamond. The mounting
495 media was allowed to cure overnight before visualization.
496 Images were acquired on a Zeiss LSM 880 Airyscan confocal microscope with a 63x objective (as
497 described for live cell imaging) by frame scanning in the superresolution mode with the following
498 settings: 35 nm x 35 nm pixel size; 80 nm z-step; 0.64 μs/pixel dwell time; 561 nm laser operating at
499 1.5% power with a 488/561 nm beam splitter, a 420-480 nm/495-620 nm band pass filter, and a gain of
500 750; 488 nm laser operating at 1.5% power with a 488/561 nm beam splitter, a 420-480 nm/495-550 nm
501 band pass filter, and a gain of 750; and 405 nm laser operating at 1.5% power with a 405 nm beam
502 splitter, a 420-480 nm/495-550 nm band pass filter, and a gain of 775.
503

Acknowledgements

Laura Wetzel, Monika Sigg, Hannah Elzinga, Lily Helfrich, and Reef Aldayafleh helped with experiments and reagent preparation. Corey Allard, as part of the Marine Biological Laboratory's Physiology Course, helped with early tests of priming conditions. Kent McDonald generously provided a transmission electron micrograph from samples prepared by Pawel Burkhardt. We thank these people for providing access and support for scientific instruments: Russell Vance and Lab for use of their luminometer, Hector Nolla and Alma Valeros in the Flow Cytometry Facility, and the UC Berkeley DNA Sequencing Facility. The following individuals generously donated reagents and provided technical support: Brad Hooks and Dee Czarniecki from Promega, Ethan Brooks from Lonza, and Colleen Manning from Zeiss. We appreciate scientific discussions and advice from these individuals: David Schaffer, Sabrina Sun, Jorge Ortiz, Niren Murthy, Tara DeBoer, Fyodor Urnov, Matt Welch and Lab, Rebecca Heald and Lab, and Abby Dernberg and Lab. We thank members of the King lab for helpful discussions, research support, and comments on the manuscript, especially Arielle Woznica, Kayley Hake, and Ben Larson. An additional thanks to the following people for providing comments on the manuscript: Candace Britton, Pawel Burkhardt, Matt Daugherty, Galo Garcia, Tera Levin, Kristin Patrick, and Dan Richter. DSB is supported as a Simons Foundation Postdoctoral Fellow of the Jane Coffin Childs Memorial Fund for Biomedical Research. This work was funded in part by a grant from the Gordon and Betty Moore Foundation's Marine Microbiology Initiative for establishing Emerging Model Systems.

Author Contributions

DSB and NK acquired funding, conceived of the project, and wrote the manuscript. DSB, HSM, and NK designed experiments and interpreted data. DSB and HSM collected data.

526 **References**

527 1. Leadbeater BSC (2015) *The Choanoflagellates: Evolution, Biology and Ecology,* (Cambridge University Press,
528 Cambridge, United Kingdom).

529 2. Fairclough SR, *et al* (2013) Premetazoan genome evolution and the regulation of cell differentiation in the
530 choanoflagellate *Salpingoeca rosetta*. *Genome Biol* 14(2): r15.

531 3. King N, *et al* (2008) The genome of the choanoflagellate *Monosiga brevicollis* and the origin of metazoans.
532 *Nature* 451(7180): 783-788.

533 4. Ruiz-Trillo I, Roger AJ, Burger G, Gray MW & Lang BF (2008) A phylogenomic investigation into the origin of
534 metazoa. *Mol Biol Evol* 25(4): 664-672.

535 5. Lang BF, O'Kelly C, Nerad T, Gray MW & Burger G (2002) The closest unicellular relatives of animals. *Curr*
536 *Biol* 12(20): 1773-1778.

537 6. Burger G, Forget L, Zhu Y, Gray MW & Lang BF (2003) Unique mitochondrial genome architecture in
538 unicellular relatives of animals. *Proc Natl Acad Sci U S A* 100(3): 892-897.

539 7. Sebe-Pedros A, Degnan BM & Ruiz-Trillo I (2017) The origin of Metazoa: A unicellular perspective. *Nat Rev*
540 *Genet* 18(8): 498-512.

541 8. Abedin M & King N (2008) The premetazoan ancestry of cadherins. *Science* 319(5865): 946-948.

542 9. Suga H, *et al* (2012) Genomic survey of premetazoans shows deep conservation of cytoplasmic tyrosine kinases
543 and multiple radiations of receptor tyrosine kinases. *Sci Signal* 5(222): ra35.

544 10. Manning G, Young SL, Miller WT & Zhai Y (2008) The protist, *Monosiga brevicollis*, has a tyrosine kinase
545 signaling network more elaborate and diverse than found in any known metazoan. *Proc Natl Acad Sci U S A*
546 105(28): 9674-9679.

547 11. Young SL, *et al* (2011) Premetazoan ancestry of the Myc-Max network. *Mol Biol Evol* 28(10): 2961-2971.

548 12. Richter D, Fozouni P, Eisen M & King N (2018) Gene family innovation, conservation and loss on the animal
549 stem lineage. *eLife* 7: e34226.

550 13. King N (2004) The unicellular ancestry of animal development. *Dev Cell* 7(3): 313-325.

551 14. King N, Hittinger CT & Carroll SB (2003) Evolution of key cell signaling and adhesion protein families
552 predates animal origins. *Science* 301(5631): 361-363.

553 15. Fairclough SR, Dayel MJ & King N (2010) Multicellular development in a choanoflagellate. *Curr Biol* 20(20):
554 875.

555 16. Levin TC & King N (2013) Evidence for sex and recombination in the choanoflagellate salpingoeca rosetta.
556 *Curr Biol* 23(21): 2176-2180.

557 17. Levin TC, Greaney AJ, Wetzel L & King N (2014) The *rosetteless* gene controls development in the
558 choanoflagellate S. rosetta. *Elife* 3: e04070.

559 18. Dayel MJ, *et al* (2011) Cell differentiation and morphogenesis in the colony-forming choanoflagellate
560 *Salpingoeca rosetta*. *Dev Biol* 357(1): 73-82.

561 19. Alegado RA, *et al* (2012) A bacterial sulfonolipid triggers multicellular development in the closest living
562 relatives of animals. *Elife* 1: e00013.

563 20. Woznica A, *et al* (2016) Bacterial lipids activate, synergize, and inhibit a developmental switch in
564 choanoflagellates. *Proc Natl Acad Sci U S A* 113(28): 7894-7899.

565 21. Woznica A, Gerdt JP, Hulett RE, Clardy J & King N (2017) Mating in the closest living relatives of animals is
566 induced by a bacterial chondroitinase. *Cell* 170(6): 1183.e11.

567 22. Helfer H & Gladfelter AS (2006) AgSwe1p regulates mitosis in response to morphogenesis and nutrients in
568 multinucleated *Ashbya gossypii* cells. *Mol Biol Cell* 17(10): 4494-4512.

569 23. Berepiki A & Read ND (2013) Septins are important for cell polarity, septation and asexual spore formation in
570 *Neurospora crassa* and show different patterns of localisation at germ tube tips. *PLoS One* 8(5): e63843.

571 24. Adam JC, Pringle JR & Peifer M (2000) Evidence for functional differentiation among *Drosophila* septins in
572 cytokinesis and cellularization. *Mol Biol Cell* 11(9): 3123-3135.

573 25. Neufeld TP & Rubin GM (1994) The *Drosophila peanut* gene is required for cytokinesis and encodes a protein
574 similar to yeast putative bud neck filament proteins. *Cell* 77(3): 371-379.

575 26. O'Neill RS & Clark DV (2013) The *Drosophila melanogaster* septin gene *Sep2* has a redundant function with
576 the retrogene *Sep5* in imaginal cell proliferation but is essential for oogenesis. *Genome* 56(12): 753-758.

577 27. Kim SK, *et al* (2010) Planar cell polarity acts through septins to control collective cell movement and
578 ciliogenesis. *Science* 329(5997): 1337-1340.

579 28. Hall MP, *et al* (2012) Engineered luciferase reporter from a deep sea shrimp utilizing a novel imidazopyrazinone
580 substrate. *ACS Chem Biol* 7(11): 1848-1857.

581 29. Janse CJ, Ramesar J & Waters AP (2006) High-efficiency transfection and drug selection of genetically
582 transformed blood stages of the rodent malaria parasite *Plasmodium berghei*. *Nat Protoc* 1(1): 346-356.

583 30. Caro F, Miller MG & DeRisi JL (2012) Plate-based transfection and culturing technique for genetic
584 manipulation of *Plasmodium falciparum*. *Malar J* 11: 22.

585 31. Vinayak S, *et al* (2015) Genetic modification of the diarrhoeal pathogen *Cryptosporidium parvum*. *Nature*
586 523(7561): 477-480.

587 32. Gresch O, *et al* (2004) New non-viral method for gene transfer into primary cells. *Methods* 33(2): 151-163.

588 33. Hamm A, Krott N, Breibach I, Blindt R & Bosserhoff AK (2002) Efficient transfection method for primary cells.
589 *Tissue Eng* 8(2): 235-245.

590 34. Rols MP & Teissie J (1990) Modulation of electrically induced permeabilization and fusion of Chinese hamster
591 ovary cells by osmotic pressure. *Biochemistry* 29(19): 4561-4567.

592 35. Rols MP & Teissie J (1989) Ionic-strength modulation of electrically induced permeabilization and associated
593 fusion of mammalian cells. *Eur J Biochem* 179(1): 109-115.

594 36. Ai HW, Henderson JN, Remington SJ & Campbell RE (2006) Directed evolution of a monomeric, bright and
595 photostable version of *Clavularia* cyan fluorescent protein: Structural characterization and applications in
596 fluorescence imaging. *Biochem J* 400(3): 531-540.

597 37. Ai HW, Olenych SG, Wong P, Davidson MW & Campbell RE (2008) Hue-shifted monomeric variants of
598 *Clavularia* cyan fluorescent protein: Identification of the molecular determinants of color and applications in
599 fluorescence imaging. *BMC Biol* 6: 13.

600 38. Pedelacq JD, Cabantous S, Tran T, Terwilliger TC & Waldo GS (2006) Engineering and characterization of a
601 superfolder green fluorescent protein. *Nat Biotechnol* 24(1): 79-88.

602 39. Shaner NC, *et al* (2013) A bright monomeric green fluorescent protein derived from *Branchiostoma*
603 *lanceolatum*. *Nat Methods* 10(5): 407-409.

604 40. Hoi H, *et al* (2013) An engineered monomeric *Zoanthus* sp. yellow fluorescent protein. *Chem Biol* 20(10): 1296-
605 1304.

606 41. Shaner NC, *et al* (2008) Improving the photostability of bright monomeric orange and red fluorescent proteins.
607 *Nat Methods* 5(6): 545-551.

608 42. Shaner NC, *et al* (2004) Improved monomeric red, orange and yellow fluorescent proteins derived from
609 *Discosoma* sp. red fluorescent protein. *Nat Biotechnol* 22(12): 1567-1572.

610 43. Yang TT, Cheng L & Kain SR (1996) Optimized codon usage and chromophore mutations provide enhanced
611 sensitivity with the green fluorescent protein. *Nucleic Acids Res* 24(22): 4592-4593.

612 44. Schiestl RH & Gietz RD (1989) High efficiency transformation of intact yeast cells using single stranded nucleic
613 acids as a carrier. *Curr Genet* 16(5-6): 339-346.

614 45. Kawai S, Hashimoto W & Murata K (2010) Transformation of *Saccharomyces cerevisiae* and other fungi:
615 Methods and possible underlying mechanism. *Bioeng Bugs* 1(6): 395-403.

616 46. Janse CJ, *et al* (2006) High efficiency transfection of *Plasmodium berghei* facilitates novel selection procedures.
617 *Mol Biochem Parasitol* 145(1): 60-70.

618 47. King N, Young SL, Abedin M, Carr M & Leadbeater BS (2009) Visualizing the subcellular localization of actin,
619 beta-tubulin, and DNA in monosiga brevicollis. *Cold Spring Harb Protoc* 2009(2): pdb.prot5150.

620 48. Sebe-Pedros A, *et al* (2013) Insights into the origin of metazoan filopodia and microvilli. *Mol Biol Evol* 30(9):
621 2013-2023.

622 49. Burkhardt P, *et al* (2014) Evolutionary insights into premetazoan functions of the neuronal protein Homer. *Mol*
623 *Biol Evol* 31(9): 2342-2355.

624 50. Kanda T, Sullivan KF & Wahl GM (1998) Histone-GFP fusion protein enables sensitive analysis of
625 chromosome dynamics in living mammalian cells. *Curr Biol* 8(7): 377-385.

626 51. Kalderon D, Roberts BL, Richardson WD & Smith AE (1984) A short amino acid sequence able to specify
627 nuclear location. *Cell* 39(3 Pt 2): 499-509.

628 52. Huh WK, *et al* (2003) Global analysis of protein localization in budding yeast. *Nature* 425(6959): 686-691.

629 53. Riedl J, *et al* (2008) Lifeact: A versatile marker to visualize F-actin. *Nat Methods* 5(7): 605-607.

630 54. Straight AF, Marshall WF, Sedat JW & Murray AW (1997) Mitosis in living budding yeast: Anaphase A but no
631 metaphase plate. *Science* 277(5325): 574-578.

632 55. Wang M & Casey PJ (2016) Protein prenylation: Unique fats make their mark on biology. *Nat Rev Mol Cell Biol*
633 17(2): 110-122.

634 56. Reid TS, Terry KL, Casey PJ & Beese LS (2004) Crystallographic analysis of CaaX prenyltransferases
635 complexed with substrates defines rules of protein substrate selectivity. *J Mol Biol* 343(2): 417-433.

636 57. Dayel MJ & King N (2014) Prey capture and phagocytosis in the choanoflagellate *Salpingoeca rosetta*. *PLoS*
637 *One* 9(5): e95577.

638 58. Friedman JR, *et al* (2011) ER tubules mark sites of mitochondrial division. *Science* 334(6054): 358-362.

639 59. Nunnari J, *et al* (1997) Mitochondrial transmission during mating in *Saccharomyces cerevisiae* is determined by
640 mitochondrial fusion and fission and the intramitochondrial segregation of mitochondrial DNA. *Mol Biol Cell* 8(7):
641 1233-1242.

642 60. Pan F, Malmberg RL & Momany M (2007) Analysis of septins across kingdoms reveals orthology and new
643 motifs. *BMC Evol Biol* 7: 103.

644 61. Nishihama R, Onishi M & Pringle JR (2011) New insights into the phylogenetic distribution and evolutionary
645 origins of the septins. *Biol Chem* 392(8-9): 681-687.

646 62. Garcia G, *et al* (2011) Subunit-dependent modulation of septin assembly: Budding yeast septin Shs1 promotes
647 ring and gauze formation. *J Cell Biol* 195(6): 993-1004.

648 63. Bertin A, *et al* (2008) *Saccharomyces cerevisiae* septins: Supramolecular organization of heterooligomers and
649 the mechanism of filament assembly. *Proc Natl Acad Sci U S A* 105(24): 8274-8279.

650 64. Sirajuddin M, *et al* (2007) Structural insight into filament formation by mammalian septins. *Nature* 449(7160):
651 311-315.

652 65. McMurray MA, *et al* (2011) Septin filament formation is essential in budding yeast. *Dev Cell* 20(4): 540-549.

653 66. Huang YW, *et al* (2008) Mammalian septins are required for phagosome formation. *Mol Biol Cell* 19(4): 1717-
654 1726.

655 67. Hu Q, *et al* (2010) A septin diffusion barrier at the base of the primary cilium maintains ciliary membrane
656 protein distribution. *Science* 329(5990): 436-439.

657 68. Ford SK & Pringle JR (1991) Cellular morphogenesis in the *Saccharomyces cerevisiae* cell cycle: Localization
658 of the CDC11 gene product and the timing of events at the budding site. *Dev Genet* 12(4): 281-292.

659 69. Kim HB, Haarer BK & Pringle JR (1991) Cellular morphogenesis in the *Saccharomyces cerevisiae* cell cycle:
660 Localization of the CDC3 gene product and the timing of events at the budding site. *J Cell Biol* 112(4): 535-544.

661 70. Cid VJ, *et al* (1998) Cell integrity and morphogenesis in a budding yeast septin mutant. *Microbiology* 144: 3463-
662 3474.

663 71. Haarer BK & Pringle JR (1987) Immunofluorescence localization of the *Saccharomyces cerevisiae* CDC12 gene
664 product to the vicinity of the 10-nm filaments in the mother-bud neck. *Mol Cell Biol* 7(10): 3678-3687.

665 72. Silverman-Gavrila RV, Hales KG & Wilde A (2008) Anillin-mediated targeting of peanut to pseudocleavage
666 furrows is regulated by the GTPase ran. *Mol Biol Cell* 19(9): 3735-3744.

667 73. Spiliotis ET, Hunt SJ, Hu Q, Kinoshita M & Nelson WJ (2008) Epithelial polarity requires septin coupling of
668 vesicle transport to polyglutamylated microtubules. *J Cell Biol* 180(2): 295-303.

669 74. Fares H, Peifer M & Pringle JR (1995) Localization and possible functions of *Drosophila* septins. *Mol Biol Cell*
670 6(12): 1843-1859.

671 75. Bowen JR, Hwang D, Bai X, Roy D & Spiliotis ET (2011) Septin GTPases spatially guide microtubule
672 organization and plus end dynamics in polarizing epithelia. *J Cell Biol* 194(2): 187-197.

673 76. Meads T & Schroer TA (1995) Polarity and nucleation of microtubules in polarized epithelial cells. *Cell Motil*
674 *Cytoskeleton* 32(4): 273-288.

675 77. Spiliotis ET (2010) Regulation of microtubule organization and functions by septin GTPases. *Cytoskeleton*
676 *(Hoboken)* 67(6): 339-345.

677 78. Spiliotis ET & Gladfelter AS (2012) Spatial guidance of cell asymmetry: Septin GTPases show the way. *Traffic*
678 13(2): 195-203.

679 79. Parra-Acero H, *et al* (2018) Transfection of *Capsaspora owczarzaki*, a close unicellular relative of animals.
680 *Development*

681 80. Suga H & Ruiz-Trillo I (2013) Development of ichthyosporeans sheds light on the origin of metazoan
682 multicellularity. *Dev Biol* 377(1): 284-292.

683 81. Li R, Neundorf I & Nitsche F (2018) First efficient transfection in choanoflagellates using cell-penetrating
684 peptides. *bioRxiv* 260190; doi: https://doi.org/10.1101/260190

685 82. Atkinson MJ & Bingman C (1998) Elemental composition of commercial seasalts. *Journal of Aquariculture and*
686 *Aquatic Sciences* 8(2): 39-43.

687 83. Hallegraeff GM, Anderson DM & Cembella AD (2004) *Manual on Harmful Marine Microalgae*. (UNESCO
688 Publishing, Paris)

689 84. Skelton HM, Burkholder JM & Parrow MW (2009) Axenic culture of the heterotrophic dinoflagellate *Pfiesteria*
690 *shumwayae* in a semi-defined medium. *J Eukaryot Microbiol* 56(1): 73-82.

691 85. Hiraoka Y, Kawamata K, Haraguchi T & Chikashige Y (2009) Codon usage bias is correlated with gene
692 expression levels in the fission yeast *Schizosaccharomyces pombe*. *Genes Cells* 14(4): 499-509.

693 86. Rice P, Longden I & Bleasby A (2000) EMBOSS: The European Molecular Biology open software suite. *Trends*
694 *Genet* 16(6): 276-277.

695 87. Harris DC (2007) *Quantitative chemical analysis,* (W.H. Freeman and Co., New York, NY),

696 88. Muranaka T, Kubota S & Oyama T (2013) A single-cell bioluminescence imaging system for monitoring
697 cellular gene expression in a plant body. *Plant Cell Physiol* 54(12): 2085-2093.

698 89. Brokaw CJ (1987) A lithium-sensitive regulator of sperm flagellar oscillation is activated by cAMP-dependent
699 phosphorylation. *J Cell Biol* 105(4): 1789-1798.

700 90. Gibbons BH & Gibbons IR (2013) Lithium reversibly inhibits microtubule-based motility in sperm flagella.
701 *Nature* 309(5968): 560-562.

702 91. Wilson KS, Gonzalez O, Dutcher SK & Bayly PV (2015) Dynein-deficient flagella respond to increased
703 viscosity with contrasting changes in power and recovery strokes. *Cytoskeleton (Hoboken)* 72(9): 477-490.

704 92. Pate EF & Brokaw CJ (1980) Movement of spermatozoa in viscous environments. *J Exp Biol* 88: 395-397.

705 93. Schindelin J, *et al* (2012) Fiji: An open-source platform for biological-image analysis. *Nat Methods* 9(7): 676-
706 682.

707 94. Cramer LP & Mitchison TJ (1995) Myosin is involved in postmitotic cell spreading. *J Cell Biol* 131(1): 179-
708 189.

709 95. Symons MH & Mitchison TJ (1991) Control of actin polymerization in live and permeabilized fibroblasts. *J Cell*
710 *Biol* 114(3): 503-513.

711 **Figure Legends**

712

713 **Figure 1: Introduction to *Salpingoeca rosetta*, an experimentally-tractable model choanoflagellate.**
714 **(A)** *S. rosetta* and other choanoflagellates are the closest living relatives of animals. Choanoflagellate is
715 abbreviated as 'Choano.'. **(B, C)** *S. rosetta* has a complex life history that includes single cells **(B)** and
716 multicellular rosettes **(C)**. Immunofluorescence in fixed, permeabilized single cells **(B)** highlights the
717 diagnostic cellular architecture of the choanoflagellate, including a single apical flagellum (f) made of
718 microtubules (white) surrounded by a collar (co) filled with F-actin (red) of microvilli. Staining for
719 tubulin also illuminates cortical microtubules (cm) that run in parallel tracks along the cell periphery from
720 the apical to the basal poles of each cell. DNA staining (blue) highlights the choanoflagellate nucleus (n)
721 and the nucleoids of bacterial prey (b) present in choanoflagellate cultures. **(C)** In multicellular rosettes
722 (stained as in panel **B**), the basal poles of cells are oriented toward the interior of the rosette and the apical
723 flagella point outward.

724

725 **Figure 2: A robust procedure for transfecting *S. rosetta***
726 **(A)** A summary of the step-wise procedure to transfect *S. rosetta* with DNA plasmids. To prepare *S.*
727 *rosetta* for transfection, cells were harvested at mid-log phase and then washed to remove bacteria
728 (depicted as grey ovals). *S. rosetta* cells (depicted with an apical collar, flagellum, and nucleus; n) were
729 primed for nucleofection (step 1) through washing with a buffer that degrades extracellular material. A
730 DNA plasmid encoding a highly sensitive luciferase, nanoluc, or a fluorescent protein (Fig. S1 and
731 Dataset 1) was then transfected into the nucleus with a nucleofector (step 2). Immediately after
732 transfection, the cells rested in a buffer that promotes membrane closure (step 3). Finally, the cells were
733 transferred into 1x High Nutrient Media prepared with AK seawater for two days (step 4) before we
734 assayed the expression of nanoluc or fluorescent proteins from transfected DNA. **(B)** Non-coding DNA
735 sequences flanking the coding sequences for *S. rosetta elongation factor L* (pEFL), *α-tubulin* (pTub), *β-*
736 *actin* (pAct), and *histone H3* (pH3) genes drive the expression of a codon-optimized *nanoluc* reporter
737 gene. 2.5 μg of pEFL-*nanoluc,* pTub-*nanoluc,* pAct-*nanoluc*, and pH3-*nanoluc* reporter plasmids were
738 each transfected into *S. rosetta* and the cells were subsequently assayed for luciferase expression. Each
739 reporter produced a luminescence signal that was at least three orders of magnitude greater than the
740 detection limit (dotted line) and significantly greater (one-way ANOVA, $p < 0.001$) than the background
741 from a negative control, in which cells were transfected with an empty pUC19 vector (None). See
742 Materials and Methods for details on replicates and statistical tests. **(C)** Systematically omitting each step
743 of the transfection procedure revealed critical steps for the delivery and expression of plasmid DNA in *S.*
744 *rosetta* cells. Transfecting cells with 2.5 μg of pH3-*nanoluc* reporter (row b) produced a luciferase signal

745 that was three orders of magnitude greater than the background detected from cells transfected without
746 the reporter plasmid (row a) and provided a baseline for comparison. Omitting the priming step by
747 incubating cells in artificial seawater instead of priming buffer (row c), decreased luciferase signal by
748 over two orders of magnitude. Nucleofection without carrier DNA (row d) or the application of the
749 CM156 electrical pulse (row e) resulted in a complete loss of luciferase signal, indicating that both were
750 essential for successful transfection. Directly transferring cells to sea water after nucleofection instead of
751 a buffer that promotes membrane resealing during the rest step (row f) decreased the luciferase signal
752 almost ten-fold. Finally, despite the fact that most prey bacteria were washed out prior to nucleofection,
753 supplementing transfected cells with fresh prey bacteria at the start of the recovery step had seemingly
754 little effect on transfection success (row g), probably due to the persistence of a small number of live
755 bacteria throughout the nucleofection procedure. **(D and E)** Fluorescent reporters mark transfected cells.
756 Live cells transfected with a pAct-m*Wasabi* reporter construct could be observed by fluorescence
757 microscopy **(D)** and quantified by flow cytometry **(E)**. Untransfected cells were used to draw a gate that
758 includes 99.99% of cells, or four-standard deviations above the mean fluorescence value (left). That same
759 gate was applied to a population of transfected cells (right) to categorize the mWasabi- population. Cells
760 with higher values of green fluorescence that lie outside of the mWasabi- gate are categorized as
761 mWasabi+. The efficiency of transformation, as quantified by three independent flow cytometry
762 experiments, was ~1% in a population of 1 million cells.
763
764 **Figure 3: Fluorescent markers illuminate the cell biology of *S. rosetta* in live cells.**
765 Fluorescent subcellular markers expressed from reporter plasmids in live *S. rosetta* cells were constructed
766 by fusing *mCherry* in frame to genes encoding localization peptides and proteins (Datasets S1 and S3).
767 Twenty-four hours after transfecting with 5 μg of each plasmid, live cells were visualized by
768 superresolution microscopy with a Zeiss LSM 880 Airyscan. In panels **A** - **I**, the cells are oriented with
769 the apical flagellum at the top and the nucleus, when included in the plane of focus (**A'' - F'')**, is
770 indicated with a dotted white line. **(A)** Without localization signals, fluorescent proteins (mCherry and
771 mTFP1) were distributed throughout the cell with a slight enrichment in the nucleus and complete
772 exclusion from other membrane bound compartments. **(B and C)** A fusion of mCherry to the carboxy
773 terminus of Histone H3 **(B)** or the amino terminus of a simian virus 40 nuclear localization signal (NLS;
774 **C)** was confined to the nucleus, whereas mCherry fused to the carboxy terminus of elongation factor L
775 (EFL; **D)** was excluded from the nucleus and restricted to the cytosol. **(E)** The endoplasmic reticulum
776 (ER) was highlighted by fusing the signal sequence from Rosetteless (PTSG_03555) and an ER retention
777 sequence (HDEL from PTSG_07223) to the amino and carboxy termini of mCherry, respectively. **(F)** The
778 mitochondrial network was highlighted by fusing a targeting sequence from *S. cerevisiae* CoxIV to the

779 amino terminus of mCherry. **(G)** A Lifeact peptide fused to the amino terminus of mCherry marked
780 filamentous actin that forms filipodia (arrowhead) and actin filaments in the cell body that coalesce to
781 form the collar (arrow). **(H)** Fusing mCherry to the amino terminus of α-Tubulin highlighted parallel
782 tracks of microtubules (arrowhead) that extended subcortically from the apical pole to the basal pole of
783 cells and microtubules that emerged from the apical pole of the cell body to form the flagellum. The
784 flagellum undulates rapidly in live cells and can be difficult to image in total; in this cell the most distal
785 tip of the flagellum is captured in the plane of focus (arrow). **(I)** A plasma membrane marker constructed
786 by fusing a geranyl-geranylation sequence (PTSG_00306) to the carboxy terminus of mCherry outlined
787 the entire cell shape, including the collar, flagellum, and cell body. The membrane marker also weakly
788 highlighted the Golgi (arrowhead). The food vacuole (asterisk) was often visualized due to
789 autofluorescence from ingested bacteria or through accumulation of the fluorescent markers in the food
790 vacuole, perhaps through autophagy. **(J - L)** Orthogonal views along the xy and xz axes from confocal
791 micrographs showed fine details of cell architecture that were highlighted with cytoskeletal and cell
792 membrane markers. In xz views, each cell is oriented with the flagellum facing toward the top of the
793 micrograph; the flagella appeared shorter and blurred because of the sigmoidal shape of the flagellar beat.
794 Lifeact **(J)** and plasma membrane **(K)** markers showed the microvilli (arrowheads). **(L)** The α-tubulin
795 marker showed the subcortical tracks of microtubules at the cell periphery (arrowhead) and the
796 microtubule organizing center (arrow).
797
798 **Figure 4: Septins assemble at the basal pole of *S. rosetta* cells.**
799 **(A)** *Sr*Septin2 has the prototypical protein domain architecture of septins, with an amino-terminal Septin
800 G-domain that mediates filament formation and a carboxy terminal coiled-coil domain that mediates
801 higher order assemblies of septin filaments. To investigate the localization of *Sr*Septin2, we engineered
802 fusions with mTFP1 at the amino terminus and created a truncation of the coiled-coil domain (ΔCC). **(B)**
803 A mTFP1-*Sr*Septin2 fusion protein localized to the basal pole of unicellular cells (**B''**, arrowhead). Co-
804 transfecting cells with mTFP1-*Sr*Septin2 and a plasma membrane marker revealed *Sr*Septin2 distributed
805 throughout the cytosol and enriched at the basal pole in confocal slices through the center of the cell. **(C)**
806 mTFP1-*Sr*Septin6 mirrored the enrichment of mTFP1-*Sr*Septin2 at the basal pole (**C''**, arrowhead). The
807 overlapping localization of *Sr*Septin2 and *Sr*Septin6 was compatible with these proteins forming
808 heteromeric filaments with each other and other septin paralogs. **(D)** Consistent with the coiled-coil
809 domain mediating the localization of septins through the formation of higher-order structures,
810 *Sr*Septin2ΔCC localized throughout the cytoplasm, with no visible enrichment at the basal pole.
811 Surprisingly, the deletion also caused ectopic filaments (**D''**; arrowheads) to form around membrane-
812 bound vesicles that were, based on their size and position in the cell, presumably food vacuoles. **(E)** In

813 rosettes, mTFP1-*Sr*Septin2 localized to points of cell-cell contact corresponding to the basal poles of cells
814 (**E''**; arrowhead). **(F)** As in single cells, mTFP1-*Sr*Septin2ΔCC in rosettes was distributed throughout the
815 cytosol and formed ectopic filaments (**F''**; arrowheads) around vacuoles. In panels **E** and **F**, *S. rosetta*
816 single cells were transfected as in panels **B** and **C**, immediately induced to develop into rosettes (20), and
817 imaged the next day. **(G)** *Sr*Septin2 intercalated between microtubules at the basal pole of the cell. Co-
818 transfecting cells with mTFP1-*Sr*Septin2 and the α-tubulin marker showed *Sr*Septin2 filaments
819 intercalated between microtubules at the basal pole in confocal slices that capture the cell cortex to easily
820 visualize microtubule tracks. (**G'**, **G''**, **G'''**; box). **G''''** shows a 4x magnification of the basal pole of a
821 representative cell (boxed region from **G'**, **G''**, **G'''**). In panels B-F, autofluorescence from ingested
822 bacteria or through accumulation of the fluorescent markers highlights the food vacuole (asterisk).

Figure 1

Introduction to *Salpingoeca rosetta*, an experimentally-tractable model choanoflagellate.

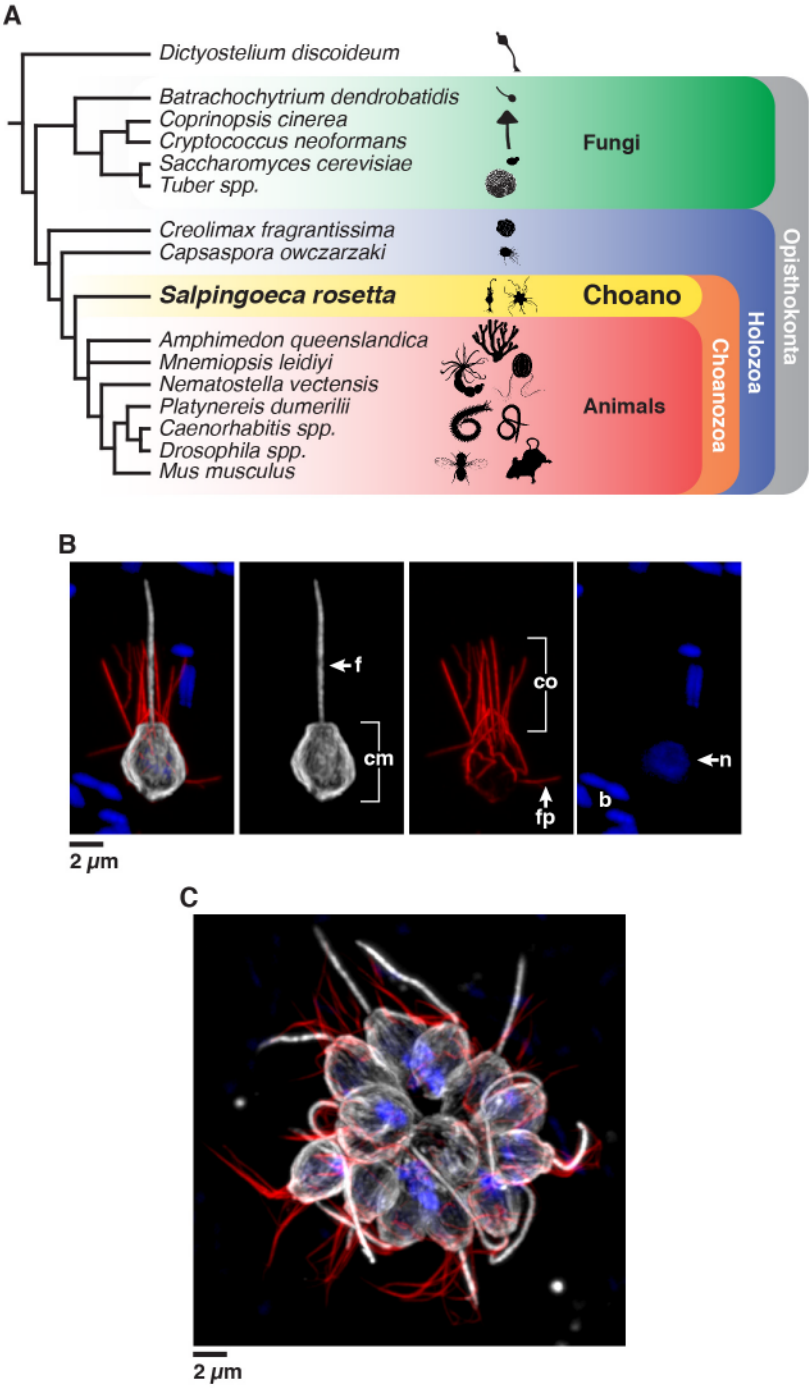

Figure 2

A robust procedure to transfect *Salpingoeca rosetta*

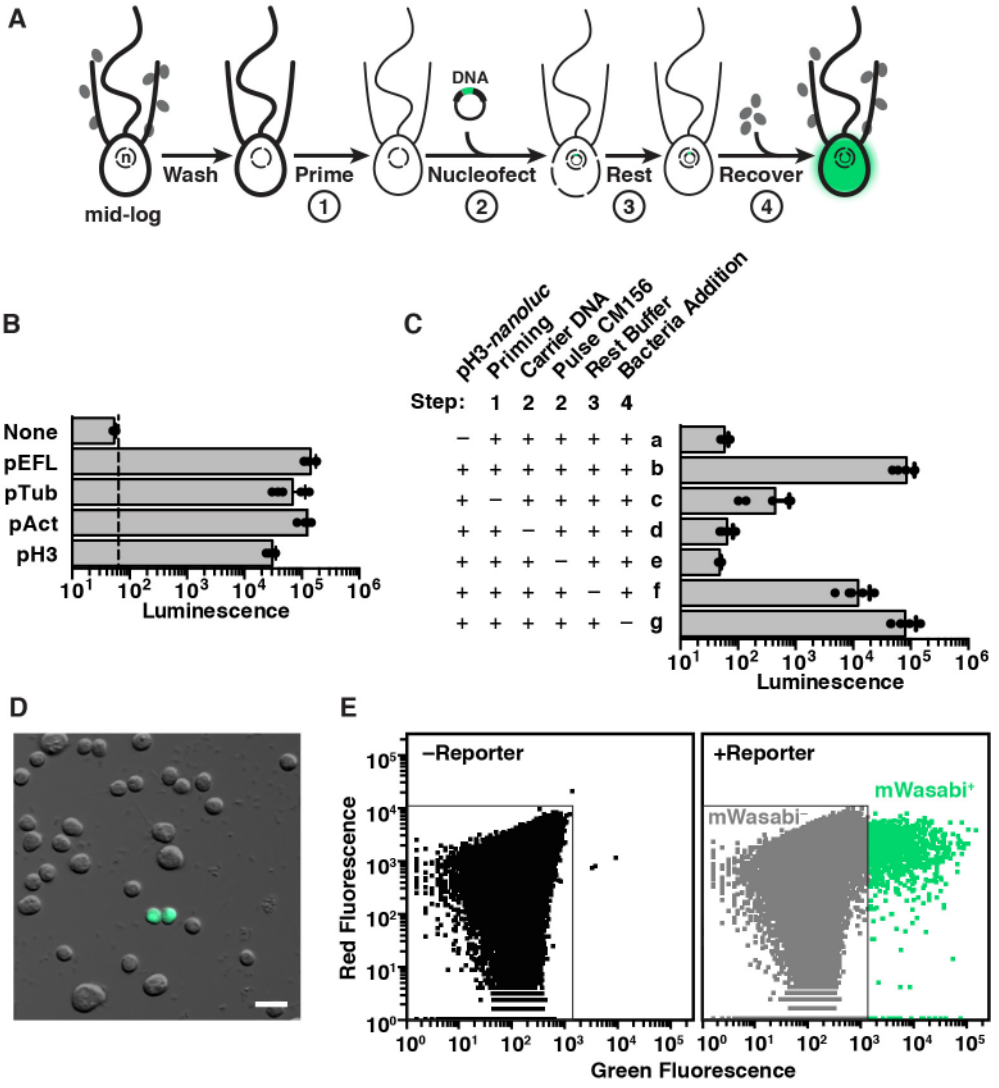

Figure 3

Fluorescent markers illuminate the cell biology of *S. rosetta* in live cells.

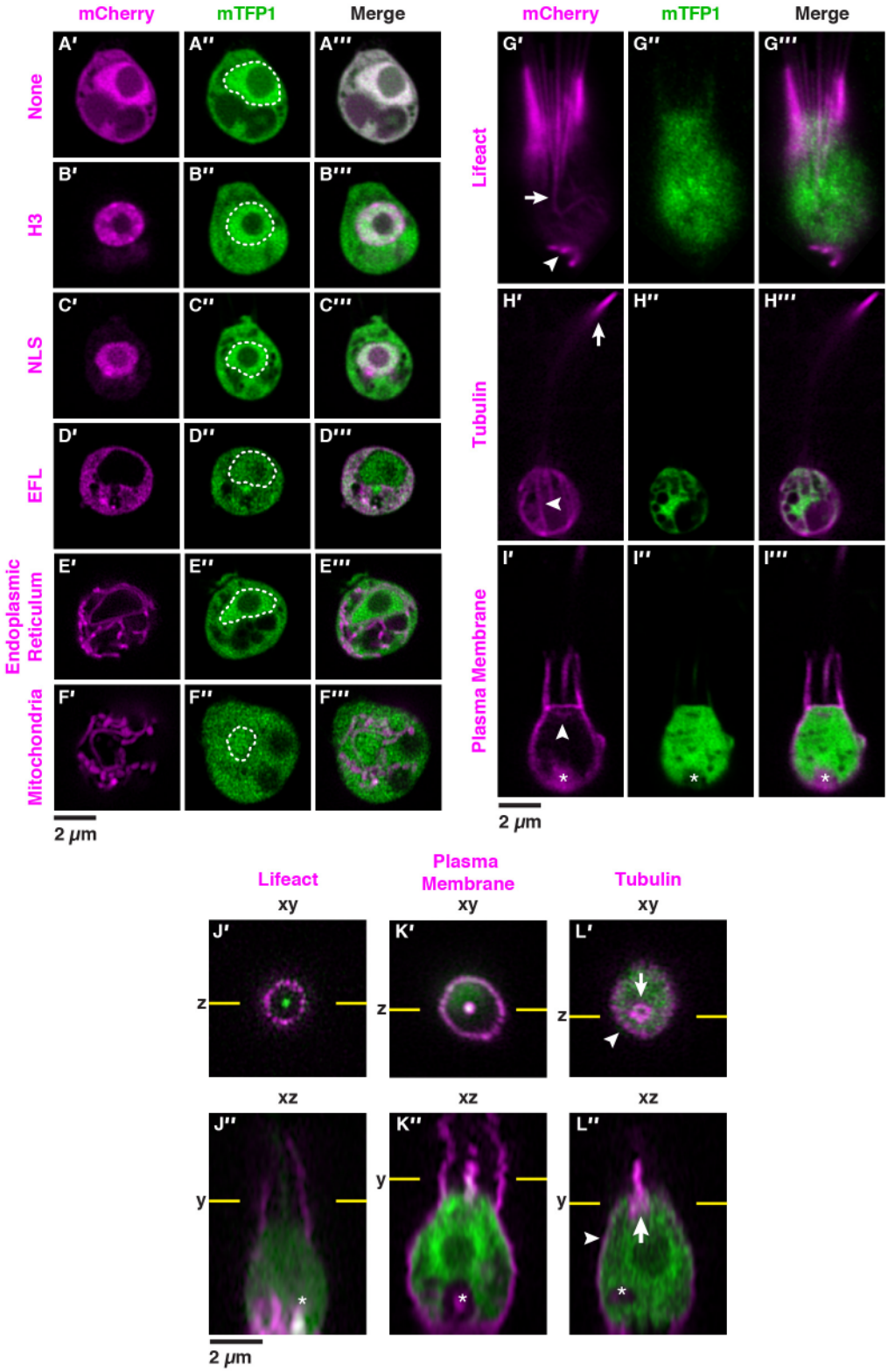

Figure 4
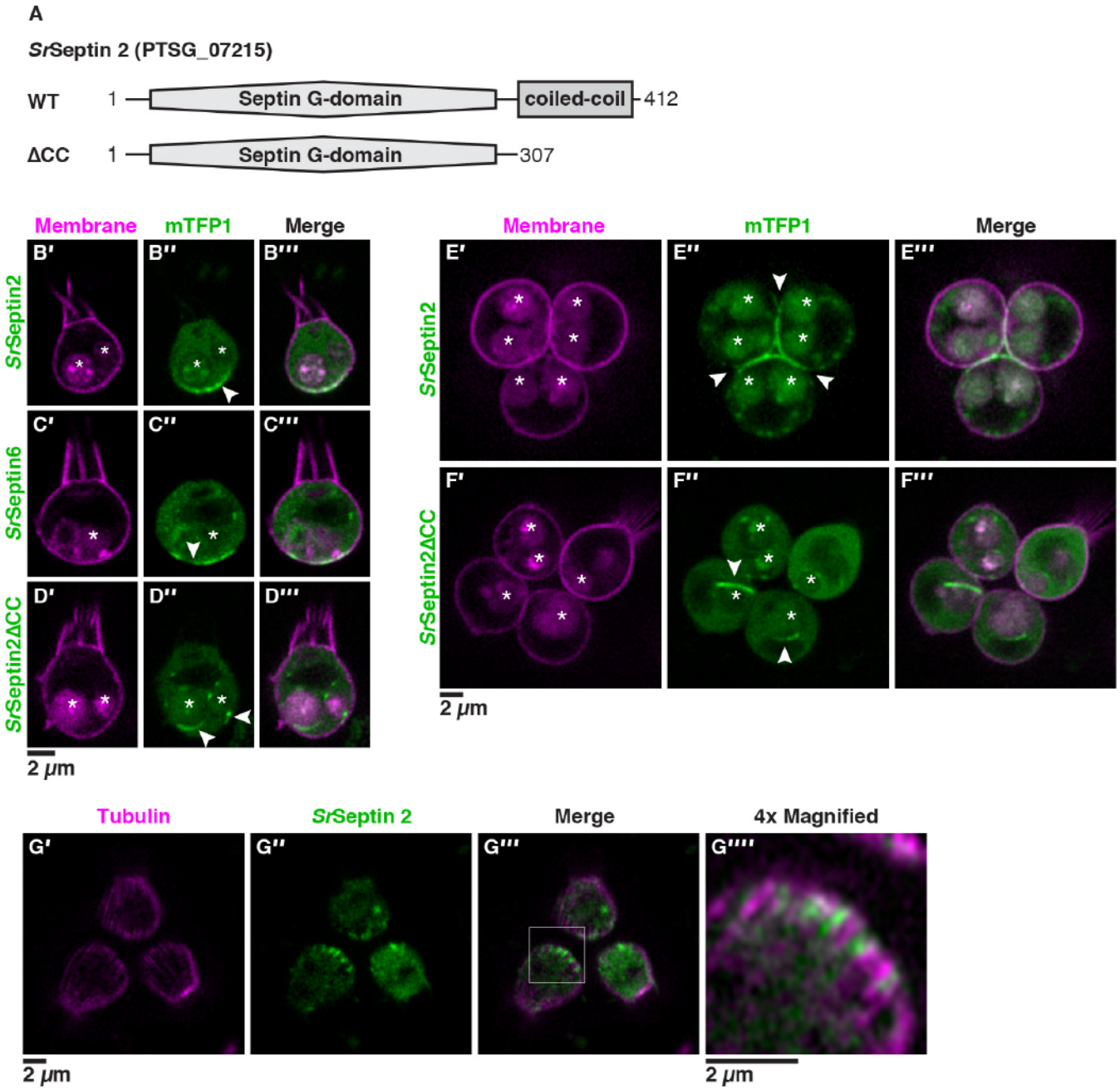
*Sr*Septin2 localizes to the basal pole of *S. rosetta* cells